JCTC Journal of Chemical Theory and Computation

Article

pubs.acs.org/JCTC

Polarizable Embedded RI-CC2 Method for Two-Photon Absorption Calculations

Dalibor Hršak,[†] Alireza Marefat Khah,[‡] Ove Christiansen,*[,†] and Christof Hättig*[,‡]

[†]Center for Oxygen Microscopy and Imaging, Aarhus University, Langelandsgade 140, 8000 Aarhus, Denmark

[‡]Lehrstuhl für Theoretische Chemie, Ruhr-Universität Bochum, Universitätsstraße 150, 44801 Bochum, Germany

Supporting Information

ABSTRACT: We present a novel polarizable embedded resolution-of-identity coupled cluster singles and approximate doubles (PERI-CC2) method for calculation of two-photon absorption (TPA) spectra of large molecular systems. The method was benchmarked for three types of systems: a water-solvated molecule of formamide, a uracil molecule in aqueous solution, and a set of mutants of the channelrhodopsin (ChR) protein. The first test case shows that the PERI-CC2 method is in excellent agreement with the PE-CC2 method and in good agreement with the PE-CCSD method. The uracil test case indicates that the effects of hydrogen bonding on the TPA of a chromophore with the nearest environment is well-described with the PERI-CC2 method. Finally, the ChR calculation shows that the PERI-CC2 method is well-suited and efficient for calculations on proteins with medium-sized chromophores.

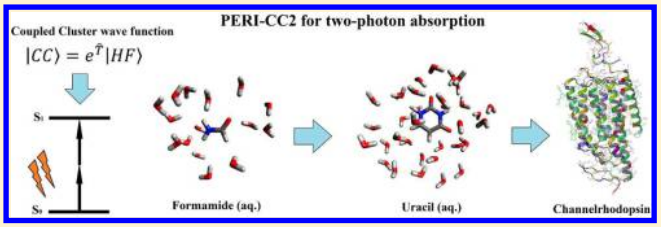

1. INTRODUCTION

Modern spectroscopy often uses multiphoton absorption processes as a very useful tool for analyzing the electronic structure of photoactive materials. Two-photon absorption[1] (TPA), where two photons are simultaneously received by a photoactive sensitizer molecule, is the most widely applied of the nonlinear absorption methods. Since its experimental confirmation,[2] TPA has found wide application in laser fluorescence microscopy,[3] photoinitiated polymerization reactions,[4] photodynamic cancer therapy,[5,6] two-photon fluorescence microscopy and deep tissue imaging,[3,7−9] two-photon microfabrication[10] and lithography,[11] optical data storage,[12] and others. The advantage of TPA compared to one-photon absorption is that is offers better spatial resolution and longer wavelength laser beams, which reduces light scattering and improves penetration into media such as biological tissues[13] without damaging the tissue itself. TPA can also experimentally find electronic transitions that are symmetry-forbidden in one-photon processes.[14]

The beneficiary features of TPA urge the development of more advanced and accurate theoretical models for instrinsic prediction of molecular sensitizers with amenable TPA spectroscopic properties. The coupled cluster[15] (CC) method has proven to be a high-accuracy method for calculating molecular properties, but the high cost of CC calculations is a limiting factor in its use. The introduction of approximations such as CC2,[16] as well as resolution-of-the-identity[17−19] (RI), enables an efficient treatment of larger molecular systems (several dozens of atoms).

A particular challenge for real chemical systems is not only the intrinsic optical or other properties of single molecules *in vacuo* but also their properties in an environment (solution, encapsulation, protein, complex, etc.). The environment can play a crucial role in enhancing desired properties. The treatment of excited states requires a sophisticated description of the interaction between a chromophore and its environment due to the change in electron density upon molecular excitation. The polarizable embedding[20−24] (PE) scheme is one such approach, which belongs to QM/MM-type methods,[25,26] and the idea behind it is similar to the effective fragment potential method (EFP),[27−29] as it divides the environment into smaller fragments (solvent molecules or amino acids of a protein) and calculates their local properties using a QM method. The atomic sites of the environment in the PE approach are assigned charges and multipoles up to a certain order, as well as polarizablities up to an order. The atomistic description of the environment provides information about the spectral broadening by sampling a set of configurations for which the excited state properties are calculated. The configurations are usually produced using an MD simulation. This makes it a more refined approach than the widely used polarizable continuum models.[30,31] The formulation of the PE scheme enables efficient derivation and implementation of response properties for molecular systems. The TPA transition matrix elements can be determined from the quadratic response function.[32] A good description of environmental effects is expected to be of particular importance for calculation of the TPA properties of complex molecular systems.[21]

In this work, we report the derivation and implementation of the PERI-CC2 method[33] for calculating TPA transition

Received: May 27, 2015
Published: July 13, 2015

DOI: 10.1021/acs.jctc.5b00496
J. Chem. Theory Comput. 2015, 11, 3669−3678

Table 1. General PE-CC Expressions for the Elements of Matrices Important for the Description of Two-Photon Transitions

	definition	vacuum contribution	PE contribution
$F_{\mu_i\nu_j}$	$\frac{\partial^2\{L^{(2)}\}_T}{\partial\bar{t}^Y_{\mu_i}(\omega_Y)\partial t^Z_{\nu_j}(\omega_Z)}$	$\langle\Lambda\vert[[\hat{H}_0, \hat{\tau}_{\mu_i}], \hat{\tau}_{\nu_j}]\vert CC\rangle$	$\langle\Lambda\vert[[\hat{G}, \hat{\tau}_{\mu_i}], \hat{\tau}_{\nu_j}] + \frac{1}{2}\hat{P}^{\mu_i\nu_j}[\hat{G}^{\mu_i}, \hat{\tau}_{\nu_j}]\vert CC\rangle$
$A_{\mu_i\nu_j}$	$\frac{\partial^2\{L^{(2)}\}_T}{\partial\bar{t}^X_{\mu_i}(\omega_X)\partial t^Y_{\nu_j}(\omega_Y)}$	$\langle\bar{\mu}_i\vert[\hat{H}_0, \hat{\tau}_{\nu_j}]\vert CC\rangle$	$\langle\bar{\mu}_i\vert[\hat{G}, \hat{\tau}_{\nu_j}] + \hat{G}^{\nu_j}\vert CC\rangle$
$F^X_{\mu_i\nu_j}$	$\frac{\partial^3\{L^{(3)}\}_T}{\partial\epsilon_X(\omega_X)\partial t^Y_{\mu_i}(\omega_Y)\partial t^Z_{\nu_j}(\omega_Z)}$	$\langle\Lambda\vert[[\hat{X}, \hat{\tau}_{\mu_i}], \hat{\tau}_{\nu_j}]\vert CC\rangle$	
$G_{\mu_i\nu_j\sigma_k}$	$\frac{\partial^3\{L^{(3)}\}_T}{\partial t^X_{\mu_i}(\omega_X)\partial t^Y_{\nu_j}(\omega_Y)\partial t^Z_{\sigma_k}(\omega_Z)}$	$\langle\Lambda\vert[[[\hat{H}_0, \hat{\tau}_{\mu_i}], \hat{\tau}_{\nu_j}], \hat{\tau}_{\sigma_k}]\vert CC\rangle$	$\langle\Lambda\vert[[[\hat{G}, \hat{\tau}_{\mu_i}], \hat{\tau}_{\nu_j}], \hat{\tau}_{\sigma_k}]\vert CC\rangle + \frac{1}{2}\hat{P}^{\mu_i\nu_j\sigma_k}\langle\Lambda\vert[[\hat{G}^{\mu_i}, \hat{\tau}_{\nu_j}], \hat{\tau}_{\sigma_k}]\vert CC\rangle$
$A^Y_{\mu_i\nu_j}$	$\frac{\partial^3\{L^{(3)}\}_T}{\partial\bar{t}^X_{\mu_i}(\omega_X)\partial\epsilon_Y(\omega_Y)\partial t^Z_{\nu_j}(\omega_Z)}$	$\langle\bar{\mu}_i\vert[\hat{Y}, \hat{\tau}_{\nu_j}]\vert CC\rangle$	
$B_{\mu_i\nu_j\sigma_k}$	$\frac{\partial^3\{L^{(3)}\}_T}{\partial\bar{t}^X_{\mu_i}(\omega_X)\partial t^Y_{\nu_j}(\omega_Y)\partial t^Z_{\sigma_k}(\omega_Z)}$	$\langle\bar{\mu}_i\vert[[\hat{H}_0, \hat{\tau}_{\nu_j}], \hat{\tau}_{\sigma_k}]\vert CC\rangle$	$\langle\bar{\mu}_i\vert[[\hat{G}, \hat{\tau}_{\nu_j}], \hat{\tau}_{\sigma_k}]\vert CC\rangle + \hat{P}^{\nu_j\sigma_k}\langle\bar{\mu}_i\vert[\hat{G}^{\nu_j}, \hat{\tau}_{\sigma_k}] + \frac{1}{2}\hat{G}^{\nu_j\sigma_k}\vert CC\rangle$
$K_{\mu_i\nu_j\sigma_k}$	$\frac{\partial^3\{L^{(3)}\}_T}{\partial\bar{t}^X_{\mu_i}(\omega_X)\partial\bar{t}^Y_{\nu_j}(\omega_Y)\partial t^Z_{\sigma_k}(\omega_Z)}$		$\hat{P}^{\mu_i\nu_j}\langle\bar{\mu}_i\vert[^{\nu_j}\hat{G}, \hat{\tau}_{\sigma_k}]\vert CC\rangle$

moments. The method is based on and inherits the efficiency of the previous implementation of RI-CC2 for excitation energies[18] and one- and two-photon[34,35] transition properties as well as the PERI-CC2 implementation[33] of excitation energies and one-photon transition properties.

The method was validated against previously reported PE methods for TPA calculations. The first system is the formamide molecule in water solution. The small size of formamide enables the excited state properties of a large number of conformations of the solute−solvent system to be easily calculated using different theoretical methods. A similar study of an aqueous solution of uracil was performed to examine the PE description of hydrogen bonding in the TPA context. The last system studied is a series of mutants of channelrhodopsin (ChR) that were considered in a previous work.[36] The chemically important part of the protein is rather large; however, it will be shown that PERI-CC2 can efficiently calculate the TPA properties of a large number of mutants. This proves the applicability of PERI-CC2 for the computational screening of the effects of mutations, thus demonstrating that it can contribute to research in optogenetics.

2. THEORY

2.1. General PE-CC Response Theory. Before defining the details of the PERI-CC2 TPA implementation, we briefly summarize the theoretical background. For further details on PE-CC theory, we refer to the literature.[23,33,37−39]

The CC wave function has an exponential *ansatz*

$$\vert CC\rangle = \exp(\hat{T})\vert HF\rangle \tag{1}$$

where $\vert HF\rangle$ is a Hartree−Fock wave function and $\hat{T}$ is the cluster operator consisting of cluster amplitudes t and excitation operators $\hat{\tau}$ in the following way

$$\hat{T} = \sum_i \hat{T}_i = \sum_{i,\mu_i} t_{\mu_i}\hat{\tau}_{\mu_i} \tag{2}$$

The index i denotes the rank of excitations such that $i = 1$ corresponds to single, $i = 2$ is for double excitations, etc. The index μ_i enumerates the excitations of the corresponding rank.

The fact that the CC state is not determined using the variational principle requires the introduction of another set of variables, named Lagrangian multipliers, $\bar{t}_{\mu_i}$. The derivation of response functions starts from the coupled cluster polarizable embedding quasi-energy Lagrangian based on the time-dependent amplitudes $\mathbf{t}(t)$ and multipliers $\bar{\mathbf{t}}(t)$

$$L^{\text{PE-CC}}(\mathbf{t}(t), \bar{\mathbf{t}}(t)) = \left\langle \Lambda\middle|\hat{H}^{\text{QM}} + \hat{G}^{\text{es}} - i\frac{\partial}{\partial t}\middle|\text{CC}\right\rangle - \frac{1}{2}\sum_{uv} F^{\text{sta},u}R^{uv}F^{\text{sta},v} + E^{\text{non-el}} \tag{3}$$

where the auxiliary $\langle\Lambda\vert$ state is

$$\langle\Lambda\vert = \left(\langle\text{HF}\vert + \sum_{i,\mu_i}\bar{t}_{\mu_i}\langle\mu_i\vert\right)\exp(-\hat{T}) \tag{4}$$

In eq 3, $\hat{G}^{\text{es}}$ describes the electrostatic interaction between the electronic density and the multipoles in the environment. $F^{\text{sta},u}$ is the static field at site u in the environment. The polarization effects are described by the second to last term, where R^{uv} is the symmetric relay matrix,[21] which describes the interaction between polarizable sites u and v. $E^{\text{non-el}}$ collects all of the terms that do not depend explicitly on CC amplitudes and Lagrangian multipliers. The static field is composed of the field from the nuclei in the QM region, the field from the QM electronic density, and the field originating from the induced moments at the other polarizable sites. The interaction of the fields with the electrons is described by the operators $\hat{e}$.

The QM Hamiltonian $\hat{H}^{\text{QM}}$ is a sum of the unperturbed QM electronic Hamiltonian $\hat{H}_0^{\text{QM}}$ and a perturbation $\hat{V}$ that can be expanded in a Fourier series

$$\hat{V} = \sum_{k=-N}^{N}\exp(-i\omega_k t)\sum_X \epsilon_X(\omega_k)\hat{X} \tag{5}$$

where $\hat{X}$ is a perturbation operator, ϵ_X is the associated strength parameter, and ω_k is the frequency of the perturbation. The perturbation is assumed to influence only the QM region. In the unperturbed case ($\hat{V} = 0$), t and $\bar{t}$ become time-independent, and the quasi-energy Lagrangian becomes the energy Lagrangian for PE-CC. In the case of no PE environment, this further reduces to the standard energy Lagrangian, which leads to standard CC energy and amplitude equations.

From the quasi-energy Lagrangian, we can determine response functions following well-known procedures.[40] The necessary quantities for CC calculation of TPA can be obtained

DOI: 10.1021/acs.jctc.5b00496
J. Chem. Theory Comput. 2015, 11, 3669−3678

from the linear and quadratic response function. The quadratic response function is obtained from the time-averaged Lagrangian of the third order in the perturbation after the application of the $2n + 1$ rule for the amplitudes and multipliers and using a fixed time-independent HF state

$$\langle\langle X; Y, Z\rangle\rangle_{\omega_Y,\omega_Z} = \frac{1}{2}\hat{C}^{\pm\omega}\hat{P}^{XYZ}\left\{\left(\frac{1}{2}\mathbf{F}^X + \frac{1}{6}\mathbf{G}\mathbf{t}^X(\omega_X)\right)\mathbf{t}^Y(\omega_Y) + \bar{\mathbf{t}}^X(\omega_X)\left(\mathbf{A}^Y + \frac{1}{2}\mathbf{B}\mathbf{t}^Y(\omega_Y)\right) + \frac{1}{2}\bar{\mathbf{t}}^X(\omega_X)\bar{\mathbf{t}}^Y(\omega_Y)\mathbf{K}\right\}\mathbf{t}^Z(\omega_Z) \tag{6}$$

$\hat{C}^{\pm\omega}$ symmetrizes the entire expression with respect to the change in sign of the frequency and complex conjugation of vectors and matrices. The matrices in the equation are defined in Table 1, separated into vacuum and PE contributions. The operator $\hat{G}$ is the effective environment operator

$$\hat{G} = \hat{G}^{es} - \sum_{uv}\langle\Lambda|\hat{\varepsilon}^u|\mathrm{CC}\rangle R^{uv}\hat{\varepsilon}^v \tag{7}$$

and its respective derivatives used in Table 1 are

$$\hat{G}^{\mu_i} = \frac{\partial\hat{G}}{\partial t_{\mu_i}} = -\sum_{uv}\langle\Lambda|[\hat{\varepsilon}^v, \hat{\tau}_{\mu_i}]|\mathrm{CC}\rangle R^{vu}\hat{\varepsilon}^u \tag{8a}$$

$${}^{\mu_i}\hat{G} = \frac{\partial\hat{G}}{\partial\bar{t}_{\mu_i}} = -\sum_{uv}\langle\bar{\mu}_i|\hat{\varepsilon}^v|\mathrm{CC}\rangle R^{vu}\hat{\varepsilon}^u \tag{8b}$$

$$\hat{G}^{\mu_i\nu_j} = \frac{\partial^2\hat{G}}{\partial t_{\mu_i}\partial t_{\nu_j}} = -\sum_{uv}\langle\Lambda|[[\hat{\varepsilon}^v, \hat{\tau}_{\mu_i}], \hat{\tau}_{\nu_j}]|\mathrm{CC}\rangle R^{vu}\hat{\varepsilon}^u \tag{8c}$$

The ground-to-excited state TPA properties can be derived from the single residues of the quadratic response function when the frequency of the external perturbation Y or Z approaches the frequency of the transition to the excited state f ($\omega_Y = \pm\omega_f$ and $\omega_Z = \pm\omega_f$). When deriving the residue of the pole, it is convenient, accurate, and, by now, standard (see refs 37, 41, and 42 for discussion) to omit the term $\mathbf{K}$. Thereby, the residues have the same form as in vacuum,[18,40] but all matrices have terms describing PE interactions. The required TPA transition moments can be derived from the cubic response function as its residues,[35] and these are the right moments

$$M^{XY}_{f\leftarrow 0} = \hat{P}^{XY}\left(L^f\left(\mathbf{A}^X + \frac{1}{2}\mathbf{B}\mathbf{t}^X\right)\mathbf{t}^Y\right) \tag{9}$$

and the left moments

$$M^{XY}_{0\leftarrow f} = \hat{P}^{XY}\left(\left(\mathbf{F}^X + \frac{1}{2}\mathbf{G}\mathbf{t}^X\right)\mathbf{t}^Y + \bar{\mathbf{t}}^X(\mathbf{A}^Y + \mathbf{B}\mathbf{t}^Y)\right)R^f + \bar{M}^f\hat{P}^{XY}\left(\mathbf{A}^X + \frac{1}{2}\mathbf{B}\mathbf{t}^X\right)\mathbf{t}^Y \tag{10}$$

The vectors L^f and R^f are the respective left and right eigenvectors of the Jacobian matrix $\mathbf{A}$. The auxiliary vector $\bar{M}^f$ depends on matrices $\mathbf{F}$ and $\mathbf{A}$

$$\bar{M}^f = -(\mathbf{F}R^f)(\omega_f\mathbf{1} + \mathbf{A})^{-1} \tag{11}$$

The matrices contained within the moments are all listed in Table 1.

2.2. Response Functions in the PERI-CC2 Form. The PE-CC calculations start from a polarizable embedding Hartree−Fock (PE-HF) calculation. This means that the mutual polarization between the environment and the quantum region is first determined fully self-consistently at the HF level. The PE-HF energy expression is in analogy to eq 3 and following ref 33 given by:

$$E^{\text{PE-HF}} = \langle\mathrm{HF}|\hat{H}_0^{\mathrm{QM}} + \hat{G}^{es}|\mathrm{HF}\rangle - \frac{1}{2}\sum_{uv}F^{\mathrm{sta},u}(\mathbf{D}^{\mathrm{HF}})R^{uv}F^{\mathrm{sta},v}(\mathbf{D}^{\mathrm{HF}}) + E^{\text{non-el}} \tag{12}$$

$F^{\mathrm{sta},u}(\mathbf{D}^{\mathrm{HF}})$ is the static field at site u including electronic effects due to the HF electron density. It is also convenient to introduce operators in their normal ordered form with respect to the HF wave function and in that way to facilitate the separation of the PE-HF terms from the correlation terms.

$$\hat{O}_N = \hat{O} - \langle\mathrm{HF}|\hat{O}|\mathrm{HF}\rangle \tag{13}$$

The ground state PE-CC quasi-energy Lagrangian can be then written as a sum of the PE-HF energy and a CC correlation contribution

$$L^{\text{PE-CC}} = E^{\text{PE-HF}} + \langle\Lambda|\hat{F}_N^{\mathrm{PE}} + \hat{V} + \hat{W}_N^{\mathrm{QM}} - i\frac{\partial}{\partial t}|\mathrm{CC}\rangle - \frac{1}{2}\sum_{uv}\langle\Lambda|\hat{\varepsilon}_N^u|\mathrm{CC}\rangle R^{uv}\langle\Lambda|\hat{\varepsilon}_N^v|\mathrm{CC}\rangle \tag{14}$$

where the QM Hamiltonian is separated into the QM Fock operator $\hat{F}^{\mathrm{QM}}$ and the QM fluctuation potential $\hat{W}^{\mathrm{QM}}$. The PE Fock operator is composed of the QM Fock operator, the electrostatic interaction operator, and the HF effective polarization contribution

$$\hat{F}^{\mathrm{PE}} = \hat{F}^{\mathrm{QM}} + \hat{G}^{es} + \hat{G}^{\mathrm{pol,HF}} \tag{15}$$

Since we use a PE-HF reference, most of the PE contributions for the unperturbed solvated system are already implicitly included through $\hat{F}^{\mathrm{PE}}$ and the PE-HF orbitals. The only contribution that one has to account for explicitly in the CC calculation is the polarization term and its response to external perturbations.

The starting point for the derivation of the PERI-CC2 Lagrangian is the PE-CCSD Lagrangian, for which a number of approximations are applied. Similar as for the vacuum CC2 model, the operator $\hat{F}^{\mathrm{PE}}$ and the singles amplitudes and multipliers are treated as zeroth order in the fluctuation potential. The operator $\hat{W}^{\mathrm{QM}}$, as well as the doubles amplitudes and multipliers, are treated as first-order quantities. The amplitude equations are then kept fully for singles, but for the doubles only the first-order terms are kept. In addition, we make two approximations in PERI-CC2 that have only a small effect on the result, but they significantly reduce the computational cost: (1) we neglect the contributions proportional to the doubles amplitudes in the last term of eq 14 so that we can recover a simple quadratic structure of *FRF*, which can be expressed with the CCS-like density,[33] and (2) we use the RI approximation (or density-fitting) for more efficient treatment of two-electron integrals in the correlation contributions. The PERI-CC2 Lagrangian accordingly has the form

DOI: 10.1021/acs.jctc.5b00496
J. Chem. Theory Comput. 2015, 11, 3669−3678

$$L^{\text{PERI-CC2}} = E^{\text{PE-HF}} + \langle \text{HF}|\hat{\tilde{V}} + \hat{\tilde{W}}_N^{\text{QM}} + [\hat{\tilde{W}}_N^{\text{QM}}, \hat{T}_2]|\text{HF}\rangle + \sum_{\mu_1} \bar{t}_{\mu_1}\langle \mu_1|\hat{\tilde{V}} + \hat{\tilde{W}}_N^{\text{QM}} + [\hat{F}_N^{\text{PE}}, \hat{T}_1] + [\hat{\tilde{V}} + \hat{\tilde{W}}_N^{\text{QM}}, \hat{T}_2] - i\frac{\partial}{\partial t}t_{\mu_1}|\text{HF}\rangle + \sum_{\mu_2} \bar{t}_{\mu_2}\langle \mu_2|\hat{\tilde{W}}_N^{\text{QM}} + [\hat{F}_N^{\text{PE}} + \hat{\tilde{V}}, \hat{T}_2] - i\frac{\partial}{\partial t}t_{\mu_2}|\text{HF}\rangle - \frac{1}{2}\sum_{uv}\langle \text{HF} + \bar{t}_1|\hat{\tilde{\varepsilon}}_N^u|\text{HF}\rangle R^{uv}\langle \text{HF} + \bar{t}_1|\hat{\tilde{\varepsilon}}_N^v|\text{HF}\rangle \tag{16}$$

To obtain a compact notation for the PERI-CC2 equations, we have introduced the $\hat{T}_1$-transformed operators, $\hat{\tilde{O}} = \exp(-\hat{T}_1)\hat{O}\exp(\hat{T}_1)$. The PE contributions from the quadratic response function appear only for matrices **G**, **B**, and **K**. In the end, matrix **K** is neglected for the purpose of TPA calculations and is therefore not implemented. Matrices **F** and **A** had their PE contributions implemented for the calculation of one-photon properties in previous work. Therefore, the only nonvanishing PE contributions that had to be implemented are those in matrices **G** and **B**

$$G^{\text{PE}}_{\mu_1\nu_1\sigma_1} = \frac{1}{2}\hat{P}^{\mu_1\nu_1\sigma_1}\langle \bar{t}_1|[[\hat{\tilde{G}}^{\mu_1}, \hat{\tau}_{\nu_1}], \hat{\tau}_{\sigma_1}]|\text{HF}\rangle \tag{17a}$$

$$B^{\text{PE}}_{\mu_1\nu_1\sigma_1} = \langle \mu_1|[[\hat{\tilde{G}}^{\Delta}, \hat{\tau}_{\nu_1}], \hat{\tau}_{\sigma_1}] + \hat{P}^{\nu_1\sigma_1}[[\hat{\tilde{G}}^{\nu_1}, \hat{\tau}_{\sigma_1}] + \hat{\tilde{G}}^{\nu_1\sigma_1}|\text{HF}\rangle \tag{17b}$$

3. IMPLEMENTATION

For the implementation, we refer to previous RI-CC2 papers for the calculation of many of the necessary RI-CC2 quantities and densities[18,35,43,44] and the previous PERI-CC2 work for integration of PE in RI-CC2.[33] In what follows, we will focus on the additional steps required for the RI-CC2 TPA implementation.

Generally, when evaluating the environment operators, we do not store the integrals for the interaction of the electrons with the individual multipole and polarizability centers because this could cause a storage bottleneck. Instead, we evaluate them whenever needed and contract them immediately with a one-electron density and the multipole moments to the environment operator $\hat{G}$ or derivatives of $\hat{G}$ contracted with the response of the cluster amplitudes and Lagrange multipliers. This strategy has a negligible effect on the overall operation count, which is dominated by the cost of the two-electron integrals, but it ensures that the disk and memory demands for the PERI-CC2 calculations are not significantly larger than those in the vacuum case.

The densities are separated into four blocks: occupied/occupied, occupied/virtual, virtual/occupied, and virtual/virtual. For convenience, occupied orbitals are denoted with indices *i*, *j*, *k*, and so on, whereas indices *a*, *b*, *c*, and so on are assigned to virtual orbitals. Indices *p*, *q*, *r*, and so on are used to denote MOs in general, without any reference to their occupancy. For evaluating the necessary PE contributions, we introduce auxiliary densities. The following densities are needed for the PE part of matrices **G** and **B**:

$$D^{\xi}_{pq}(L) = \sum_{\mu_1} L_{\mu_1}\langle \mu_1|\hat{E}_{pq}|\text{HF}\rangle \tag{18a}$$

$$D^{\eta}_{pq}(R) = \sum_{\mu_1} \langle \text{HF} + \bar{t}_1|[\hat{E}_{pq}, \hat{\tau}_{\mu_1}]|\text{HF}\rangle R_{\mu_1} \tag{18b}$$

$$D^{A}_{pq}(L, R) = \sum_{\mu_1\nu_1} L_{\mu_1}\langle \mu_1|[\hat{E}_{pq}, \hat{\tau}_{\nu_1}]|\text{HF}\rangle R_{\nu_1} \tag{18c}$$

$$D^{F}_{pq}(R^X, R^Y) = \sum_{\mu_1\nu_1} \langle \bar{t}_1|[[\hat{E}_{pq}, \hat{\tau}_{\mu_1}], \hat{\tau}_{\nu_1}]|\text{HF}\rangle R^X_{\mu_1}R^Y_{\nu_1} \tag{18d}$$

$$D^{B}_{pq}(L, R^X, R^Y) = \sum_{\mu_1\nu_1\sigma_1} L_{\mu_1}\langle \mu_1|[[\hat{E}_{pq}, \hat{\tau}_{\nu_1}], \hat{\tau}_{\sigma_1}]|\text{HF}\rangle R^X_{\nu_1}R^Y_{\sigma_1} \tag{18e}$$

The $\hat{T}_1$-transformation of the operators gives an opportunity to introduce the $\hat{T}_1$-transformed integrals $\tilde{x}_{pq}$. The densities in eqs 18 are defined for a $\hat{T}_1$-transformed MO basis, for which the MO integrals are given in terms of the AO integrals

$$\tilde{x}_{pq} = \sum_{\sigma\rho} \Lambda^p_{\rho p}\Lambda^h_{\sigma q}x_{\rho\sigma} \tag{19}$$

where ρ and σ are AO indices and $\Lambda^p = \mathbf{C}(\mathbf{1} - \mathbf{t}_1^{\text{T}})$ and $\Lambda^h = \mathbf{C}(\mathbf{1} + \mathbf{t}_1)$ are the occupied and virtual transformation matrices, respectively.

The elements of the density matrices are listed in Table 2. At this point, it is possible to find computationally tractable

Table 2. Elements of the CCS-Like Density Matrices Used To Evaluate the Response of the Environment Potential $\hat{G}$ to Changes in the Amplitudes and Multipliers

density	D_{ij}	D_{ai}	D_{ia}	D_{ab}
$\mathbf{D}^{\xi}(L)$	0	L_{ai}	0	0
$\mathbf{D}^{\eta}(R)$	$-\sum_a \bar{t}_{aj}R_{ai}$	0	$2R_{ai}$	$\sum_i \bar{t}_{ai}R_{bi}$
$\mathbf{D}^{A}(L, R)$	$-\sum_a L_{aj}R_{ai}$	0	0	$\sum_i L_{ai}R_{bi}$
$\mathbf{D}^{F}(R^X, R^Y)$	0	0	$-\hat{P}^{XY}\sum_{bj}\bar{t}_{bj}R^X_{aj}R^Y_{bi}$	0
$\mathbf{D}^{B}(L, R^X, R^Y)$	0	0	$-\hat{P}^{XY}\sum_{bj}L_{bj}R^X_{aj}R^Y_{bi}$	0

expressions for matrices **G** and **B** transformed with two or three vectors. Matrix **G** can be contracted with three right auxiliary vectors, so its PE contribution to eq 10 becomes

$$\begin{aligned}\sum_{\mu_1\nu_1\sigma_1} G^{\text{PE}}_{\mu_1\nu_1\sigma_1}R^X_{\mu_1}R^Y_{\nu_1}R^Z_{\sigma_1} &= \hat{P}^{XYZ}\langle \bar{t}_1|[[\hat{\tilde{G}}^{\Delta}(\mathbf{D}^{\eta}(R_1^X)), R_1^Y], R_1^Z]|\text{HF}\rangle \\ &= -\hat{P}^{XYZ}\sum_{ia}\sum_{bj}(\bar{t}_{bi}\tilde{G}^{\Delta}_{ja}(\mathbf{D}^{\eta}(R_1^X)) \\ &\quad + \bar{t}_{aj}\tilde{G}^{\Delta}_{ib}(\mathbf{D}^{\eta}(R_1^X)))R^Y_{bj}R^Z_{ai}\end{aligned} \tag{20}$$

with the correlated polarization term for a given CCS-like density **D** being $\hat{\tilde{G}}^{\Delta}(\mathbf{D}) = -\sum_{uv}\hat{\varepsilon}^u R^{uv}\text{Tr}(\tilde{\boldsymbol{\varepsilon}}^v\mathbf{D})$.

The matrix **B** is contractd with one left and one right auxiliary vector to evaluate its contributions in eqs 9 and 10. When written out in a form appropriate for implementation, this transformation becomes

DOI: 10.1021/acs.jctc.5b00496
J. Chem. Theory Comput. 2015, 11, 3669−3678

$$\sum_{\mu_1\nu_1} L_{\mu_1} B^{\mathrm{PE}}_{\mu_1\nu_1\sigma_1} R_{\nu_1} = \langle L_1|[[\hat{\tilde{G}}^{\Delta}(\mathbf{D}^{\Delta}), R_1], \hat{\tau}_{\sigma_1}]|\mathrm{HF}\rangle + \langle L_1|[\hat{\tilde{G}}(\mathbf{D}^{\eta}(R_1)), \hat{\tau}_{\sigma_1}]|\mathrm{HF}\rangle + \langle \mathrm{HF} + \bar{t}_1|[\hat{\tilde{G}}^{\Delta}(\mathbf{D}^{A}(L_1, R_1)), \hat{\tau}_{\sigma_1}]|\mathrm{HF}\rangle + \langle \bar{t}_1|[[\hat{\tilde{G}}^{\Delta}(\mathbf{D}^{\xi}(L_1)), R_1], \hat{\tau}_{\sigma_1}]|\mathrm{HF}\rangle$$
$$= -\sum_{bj} L_{bi}\tilde{G}^{\Delta}_{ja}(\mathbf{D}^{\Delta})R_{bj} - \sum_{jb} L_{aj}\tilde{G}^{\Delta}_{ib}(\mathbf{D}^{\Delta})R_{bj} + \sum_{b} L_{bi}\tilde{G}^{\Delta}_{ba}(\mathbf{D}^{\eta}(R_1)) - \sum_{j} L_{aj}\tilde{G}^{\Delta}_{ij}(\mathbf{D}^{\eta}(R_1)) + 2\tilde{G}^{\Delta}_{ia}(\mathbf{D}^{A}(L_1, R_1)) + \sum_{b} \bar{t}_{bi}\tilde{G}^{\Delta}_{ba}(\mathbf{D}^{A}(L_1, R_1)) - \sum_{j} \bar{t}_{aj}\tilde{G}^{\Delta}_{ij}(\mathbf{D}^{A}(L_1, R_1)) - \sum_{bj} \bar{t}_{bi}\tilde{G}^{\Delta}_{ja}(\mathbf{D}^{\xi}(L_1))R_{bj} - \sum_{jb} \bar{t}_{aj}\tilde{G}^{\Delta}_{ib}(\mathbf{D}^{\xi}(L_1))R_{bj} \quad (21)$$

The polarization contributions are then added to the contractions of matrices **G** and **B**, needed for evaluation of the transition moments. These matrices are implemented in the local development version of the Turbomole package,[45] based on release V6.6.

4. CALCULATIONS

Three systems were chosen to illustrate the performance of the implemented method: a water-solvated formamide molecule, a water-solvated uracil molecule, and a series of mutants of the ChR protein. In the first example, the PERI-CC2 method was benchmarked for TPA against well-documented previous implementations of PE-CC methods for TPA. In the case of uracil, the PERI-CC2 description of the influence of hydrogen bonding on TPA was analyzed. The last example has been used to depict the efficiency and accuracy of the PERI-CC2 method in the calculation of TPA properties of a protein with a large photoactive site.

4.1. Aqueous Solution of Formamide. Formamide is a small molecule well-suited for a large number of calculations using different computational methods. In this case, the TPA calculations were performed on 120 snapshots of a water-solvated formamide molecule. The details of the preparation procedure of the snapshots and embedding potential calculations can be found in a previous study.[23] The embedding potential describing the solvating water molecules includes multipoles up to quadrupoles and anisotropic polarizabilities. The results from the PERI-CC2 calculations were compared with the results from the calculations performed using PE-CC2 and PE-CCSD methods that were previously implemented in the Dalton program.[46] In all calculations, the aug-cc-pVDZ[47] basis set was used. For PERI-CC2, a large auxiliary basis set, aug-cc-pV6Z,[48−50] was used to minimize the error that arises from the RI approximation. The primary difference between PE-CC2 and PERI-CC2 is, therefore, not the RI approximation of two-electron integrals *per se* but the special approximation of the PE response term; PERI-CC2 uses the CCS-like density, whereas PE-CC2 uses the full CC2 density. In vacuum, the formamide molecule was optimized at the B3LYP/aug-cc-pVTZ level of theory using Gaussian 09,[51] and its TPA spectrum was calculated using the RI-CC2 method with the same basis sets as those for PERI-CC2.

Properties of the first four vertically excited states of the formamide molecule surrounded by 248 PE water molecules were calculated. The variations of calculated TPA transition probabilities (δ^{TPA}) throughout the snapshots are shown in Figure 1. The values of δ^{TPA} were convoluted in a Lorentzian-type shape function as described elsewhere,[52] and the full-width-at-half-maximum (fwhm) was set to 0.2 eV. The simulated TPA spectrum calculated with all three methods is shown in Figure 2a.

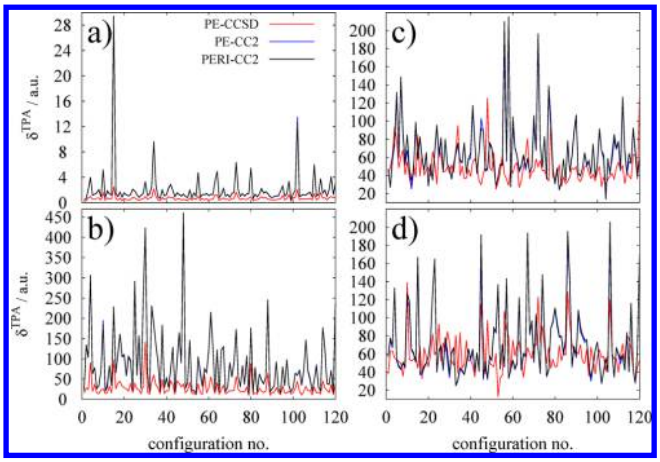

Figure 1. Comparison of TPA transition probabilities of the aqueous solution of formamide throughout 120 snapshots calculated using PE-CCSD, PE-CC2, and PERI-CC2 for the first (a), second (b), third (c), and fourth (d) excited states.

The PERI-CC2 results are in almost perfect agreement with the PE-CC2 results, visible from the fact that the lines for PERI-CC2 and PE-CC2 in the spectra nearly completely overlap. This holds not only on average, as in Figure 2, but also for each snapshot individually, as shown in Figure 1. As expected, the PE-CCSD method yielded somewhat different results for excitation energies and TPA cross-sections. The spectral maxima for PERI-CC2 and PE-CC2 are red-shifted by about 0.2 eV from the PE-CCSD peak, and the PE-CCSD peak is lower by about 0.5 Göppert-Mayer (GM) units. This indicates that the main differences between the PE-CCSD and PERI-CC2 methods have their origin in the CC2 approximation of the doubles excitations manifold.

The large peak corresponds to the intensive transition from the ground to the second, third, and, to a lesser extent, fourth excited states, depending on the snapshot. The fourth excited state also appears as a weak shoulder on the right-hand side of the intensive peak. The first excited state corresponds to a very weak transition in the range from ∼6.1 to ∼6.9 eV (depending on the snapshot), and it is not visible in the spectrum. It is also visible from Figure 1 that the largest difference in TPA between the CCSD- and the CC2-based approaches arises in the second excited state, where the PE-CCSD values of δ^{TPA} are visibly lower than the PE-CC2 and PERI-CC2 values.

Regarding the nature of the excited states, the first excited state exhibits clear features of the $n \rightarrow \pi^*$ transition. The other three excited states are a mixture of valence states produced by $\pi \rightarrow \pi^*$ transitions and Rydberg-type states. The complicating circumstance for this system is that the nature of these three states clearly varies throughout the snapshots for both CC2-

DOI: 10.1021/acs.jctc.5b00496
J. Chem. Theory Comput. 2015, 11, 3669−3678

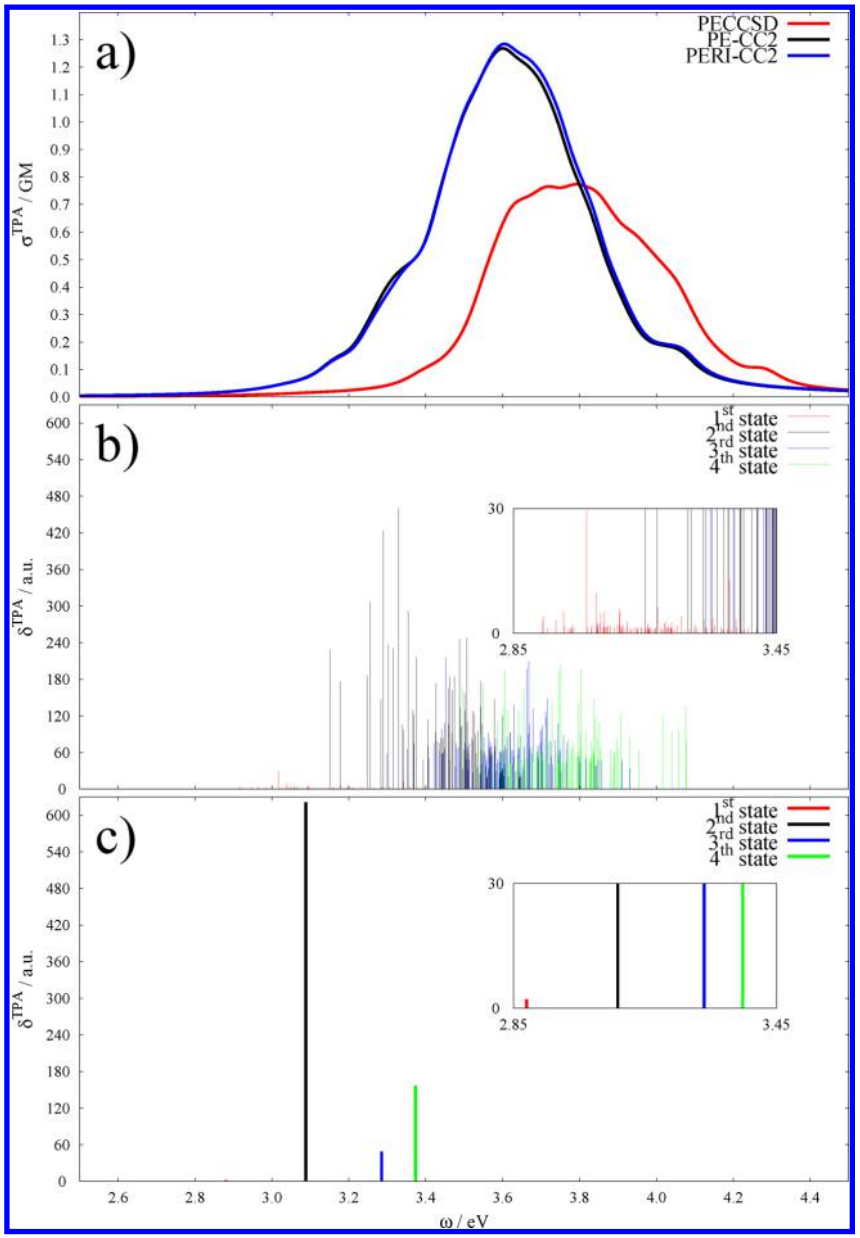

Figure 2. (a) TPA cross-section (σ^{TPA}) of a water-solvated formamide molecule as a function of the laser frequency (ω) calculated with PE-CCSD, PE-CC2, and PERI-CC2 methods, (b) TPA stick spectra of 120 snapshots of a water-solvated formamide molecule calculated with PERI-CC2 and (c) TPA stick spectrum of the formamide molecule in vacuum calculated with RI-CC2.

based methods, but it does not vary that much for PE-CCSD. This explains the large fluctuations in δ^{TPA} values for PE-CC2 and PERI-CC2 seen in Figure 1. The slight difference in behavior for PE-CCSD and PERI-CC2/PE-CC2 is thus attributed to somewhat larger errors for the Rydberg transitions for CC2 compared to CCSD. The RI approximation, however, does not seem to be affected by the presence of Rydberg states, as was also found in previous vacuum work.[35]

Large fluctuations in δ^{TPA} for this case also imply the need for a large number of configurations (approximately 100 or more) in order to obtain a statistically relevant sample for averaging. It can be seen from the results included in the Supporting Information that a small set (30 points) yields an erroneous spectrum, but a gradual increase in the number of configurations improves the result and for 90 points and more changes are small, in particular for the peak maximum value and position.

For comparison, the OPA spectrum (in the Supporting Information) exhibits much less difference between PE-CCSD and PERI-CC2, which implies that the description of the nonlinear absorption depends much more strongly on the inclusion of doubles amplitudes than linear absorption. The reason for this probably lies in the fact that in CC response theory the doubles amplitudes describe not only correlation effects and the physical excitation processes but also partially the response of the correlated and uncorrelated parts of the wave function to the electric fields. In difference to the OPA moments, the TPA moments depend explicitly on the first-order responses of the ground state wave function and might, for this reason, be more sensitive to approximations in the doubles amplitudes.

Water solvation produces a blue shift for all four excited states, as visible in Figure 2b,c. The δ^{TPA} value is significantly higher in vacuum than in solution for the second excited state,

DOI: 10.1021/acs.jctc.5b00496
J. Chem. Theory Comput. 2015, 11, 3669−3678

it is lower for the third excited state, and it is higher than most PE snapshots for the fourth excited state. For the first excited state, there is generally no significant difference in δ^{TPA} for vacuum and PE, as it is an extremely weak transition.

4.2. Uracil in Water. The second analyzed system was the water solution of a uracil molecule, a pyrimidine nucleobase that naturally occurs in ribonucleic acid (RNA), where it forms double hydrogen bonds with adenine. An accurate description of interaction of nucleobases with light is needed for further elucidation of the process of photoinduced damage of nucleic acids.[53,54] The UV−vis spectrum of uracil in gas phase and solution has been a target of myriad experimental and theoretical studies.[55−63] However, the literature on two-photon properties of nucleobases does not seem to be abundant.

The water solution of uracil was described using two models: model 1, where only the uracil molecule was included in the QM region and all of the solvating water molecules were described with PE, and model 2, where four water molecules hydrogen-bonded with uracil were included in the QM region and the rest of the solvating system was described with PE. This analysis gave insight into the accuracy of the PE description of the influence of hydrogen bonding on TPA transition probabilities and the positions of band maxima in the PERI-CC2 context. The applied basis set was aug-cc-pVDZ, along with the aug-cc-pV6Z auxiliary basis set; the large auxiliary basis set minimizes the error arising from the RI approximation in the PERI-CC2 model. The first two excited states were calculated for 120 snapshots generated from an MD simulation. The first excited state corresponds to a $\pi \rightarrow \pi^*$ transition, and the second excited state, to a $n \rightarrow \pi^*$ transition. The order of these two states is reversed in vacuum,[59] and this reversal has been found in other studies as well.[64] The details of the applied computational procedure for MD can be found elsewhere.[62] The obtained spectra of 120 snapshots were convoluted in a Lorentzian shape function and averaged to produce a single spectrum. The fwhm value is set to be 0.2 eV. Using 120 snapshots for uracil ensures that a reliable spectral simulation is attained, as for formamide, although for uracil, this can already be achieved with 60 snapshots, as shown in the Supporting Information.

Figure 3 shows the TPA spectra for the two approaches. Both spectra show one distinct and strong band. The maximum TPA cross-section for both approaches is at a laser frequency of 2.58 eV, which corresponds to an excitation energy of 5.16 eV. Our predicted OPA band maximum for the two models is also at 5.16 eV, which is 0.37 eV higher than the experimental result (4.79 eV for the OPA spectrum).[56,60] The maximum TPA cross-section is higher by ∼0.1 GM unit for model 2 than for model 1 with the given fwhm. This strong band corresponds to the $\pi \rightarrow \pi^*$ transition. The weak $n \rightarrow \pi^*$ transition is located at 5.51 eV for model 1 and at 5.43 eV for model 2. Since the second transition is not visible from the spectrum, its position for the two models was retrieved as the averaged excitation energy of the second singlet excited state of the 120 snapshots.

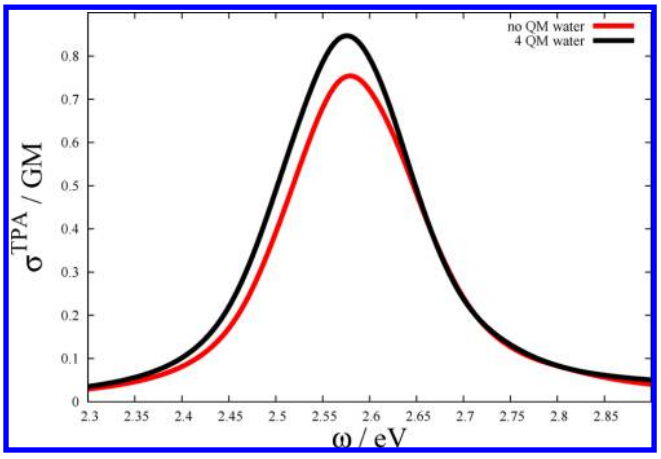

Figure 3. TPA cross-section (σ^{TPA}) of a water-solvated uracil molecule as a function of the laser frequency (ω) without and with four hydrogen-bonded water molecules in the QM region.

The analysis indicated that the additional four hydrogen-bonded water molecules in the QM region produce only slight differences in the TPA spectrum and that the PE approach provides a very good description of the influence of hydrogen bonding on TPA transition strengths. On the other hand, the inclusion of additional four water molecules into the QM region increases the computational problem (from 236 to 408 basis functions and from 21 to 37 occupied valence orbitals), which leads, approximately, to a 10-fold increase in computational time. The benefits of this improvement in the description of the system are only marginal, considering the magnitude of other errors involved.

4.3. Large-Scale Application: Channelrhodopsin. ChR is a photoactive transmembrane protein found in algae *Chlamydomonas reinhardtii*.[65−67] It has been a key system suitable for optogenetic research,[68] and a number of its variants and mutants have been experimentally scrutinized.[69,70] Large two-photon cross-sections have also been reported.[71] The reason for choosing this system is 2-fold: (a) a previous study of a series of pertinent point mutants[36] allowed us to make a comparison with already existing data and (b) the size of its chromophore makes a TPA study of a large number of mutants using high-accuracy theoretical models a challenging task. It shall be shown in this study that it is computationally tractable to calculate TPA properties of ChR with the PERI-CC2 model.

A calculation of one mutation took about 220 h of wall-clock time on eight processors (Intel/Nehalem X5550, 2.6 GHz), which is computationally demanding but not unfeasible with available resources. There are no other computational times available for comparison with PERI-CC2, and a PE-CC2 calculation would be unrealistic and inefficient for a large set of ChR mutations. This can be attributed to the fact that the RI approximation reduces the RI-CC2 operation count from $O(nN^4)$ to $O(n^2N^3)$, where n is the number of electrons and N is the number of basis functions. This typically leads to a reduction by 1 or 2 orders of magnitude in computational time for both vacuum and PE calculations.

The computational procedure was the same as that indicated in the previous study by Sneskov et al.,[36] and it included the same chimeral C1C2 variant[72,73] and the same set of mutants of C1C2. Only one fixed molecular configuration per mutation was used for the calculations. This introduced an error, namely, no dynamic effects are taken into consideration and the peaks for the transitions have no spectral width, as in experimental spectra or computational spectra of snapshots generated using MD simulations. On the other hand, using such MD sampling would increase the number of calculations from one to at least 30 per mutation (not taking the MD simulation and QM/MM optimization into account), making it much more costly to screen a large set of different mutants.

The first series of mutations included those for which experimental and computational results for TPA properties are

DOI: 10.1021/acs.jctc.5b00496
J. Chem. Theory Comput. 2015, 11, 3669−3678

Table 3. Spectral Shifts and Relative Differences in TPA Transition Probabilities of ChR Mutants with Respect to Wild-Type ChR and Comparison with Previous Computational (PE-TDDFT) and Experimental Results

	$(\lambda_{mut} - \lambda_{wt})$/nm			$((\delta_{mut}^{TPA} - \delta_{wt}^{TPA})/\delta_{wt}^{TPA}) \times 100\%$	
mutant	PERI-CC2	PE-TDDFT[36]	exp[74,75]	PERI-CC2	PE-TDDFT[36]
T198C	3.5	3	0	18	20
T198C + E162T	50.8	28	35	161	150
H173R	−6.8	0	0	0.5	0
E162A	45.7	25	20	133	120
E162D	10.1	6	10	27	30
E162Q	67.2	37	30	186	160
E162T	42.2	23	30	124	120

already available. The TPA results of the first series of pertinent mutants are shown in Table 3. The combined mutation T198C/E162T and a single mutation E162Q give the largest red shift in the excitation energy and provide the best enhancement in the TPA properties. H173R, on the other hand, yields deterioration of the TPA properties. This result is in agreement with previous results and confirms predictions of the PE-TDDFT study.[36]

Another series included a set of point mutations of different amino acids to glycine (G). The result showed that changing amino acids that are closest to the chromophore has the largest influence on both the spectral shifts and the TPA transition probabilities (Figure 4). Although the distance from the chromophore plays a crucial role in the extent of the influence of mutation on the TPA transition probabilities, there are still several mutations that have an unusually large effect compared to that for other mutations at sites of comparable distances. These correspond to mutations from positively or negatively charged amino acids (lysine (K), glutamate (E), and arginine (R)) to G and from tryptophan (W) and serine (S) to G. Whereas substitution of W and K with G yields deterioration of the TPA properties, substitutions of S and R enhance TPA. Interestingly, substitutions of two different E residues (122 and 274) produce the opposite effect on the TPA properties of the protein. There is no indication why this would be the case.

The last series consisted of a set of point mutations of E162 to various amino acids. Glutamate is an amino acid with a negatively charged side chain. As visible from Figure 5, it seems that the largest enhancement in TPA properties takes place upon mutation from E to an amino acid with a positively charged side chain, like K or R. The previous study (PE-TDDFT) predicted less TPA enhancement for the E162K mutant than for E162R, whereas PERI-CC2 predicts that the E162K mutation would have a larger TPA transition probability than that for E162R. This observation is also in line with the fact that E162K has the largest red spectral shift. E162Q also exhibits a significant enhancement in the TPA properties, whereas other mutations all exhibit nearly the same extent of spectral shifts and changes in TPA transition probabilities. The smallest difference in TPA properties relative to those of the wild-type protein is exhibited by the E162D mutant, which is also expected because aspartate (D) is the amino acid most similar to E.

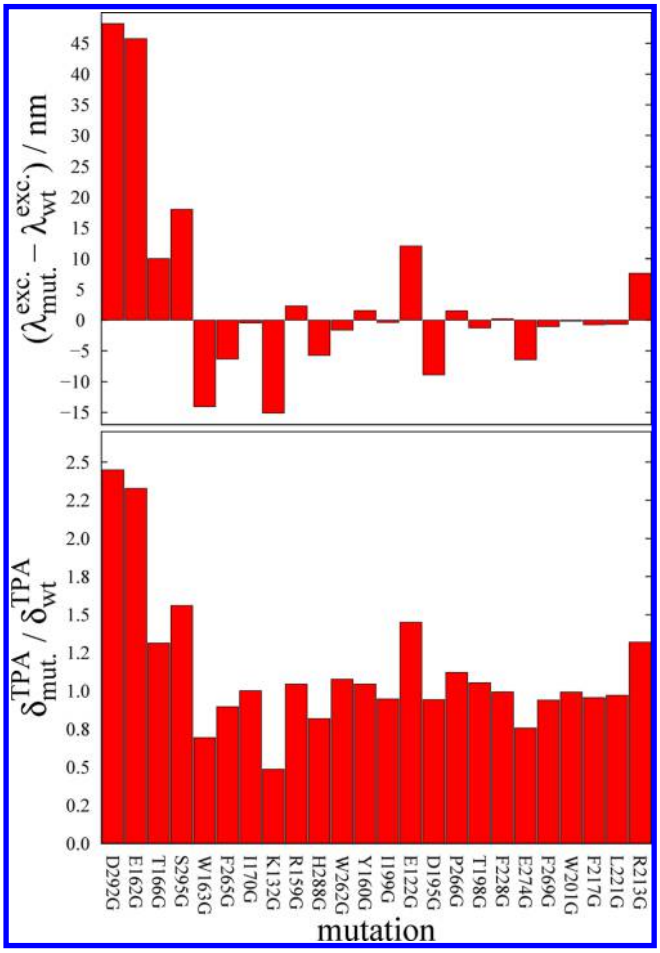

Figure 4. Spectral shifts (up) and TPA transition probability ratios (down) with respect to the wild-type protein for a series of amino acid-to-glycine mutations, ordered with respect to the distance from the Schiff-base of the chromophore.

5. CONCLUSIONS

In this work, we extended the PERI-CC2 method to the calculation of TPA spectra of large molecular systems and presented an implementation of it in the Turbomole package for quantum chemistry. This method enables significantly more efficient computational predictions of TPA spectra with a CC method than were possible before.

It is shown in the case of formamide that the PERI-CC2 method provides virtually the same results as those with the previously implemented PE-CC2 method but with much less computational effort. This justifies the use of CCS-like densities for the polarization. The PE approach likewise satisfactorily describes the influence of hydrogen bonding on the TPA of a chromophore with little additional computational effort, as shown in the example of uracil. In the last example, the PERI-CC2 method was applied on a series of mutants of the ChR protein. The active site in the protein is quite large (66 atoms), yet the PERI-CC2 method successfully managed to fulfill the

DOI: 10.1021/acs.jctc.5b00496
J. Chem. Theory Comput. 2015, 11, 3669−3678

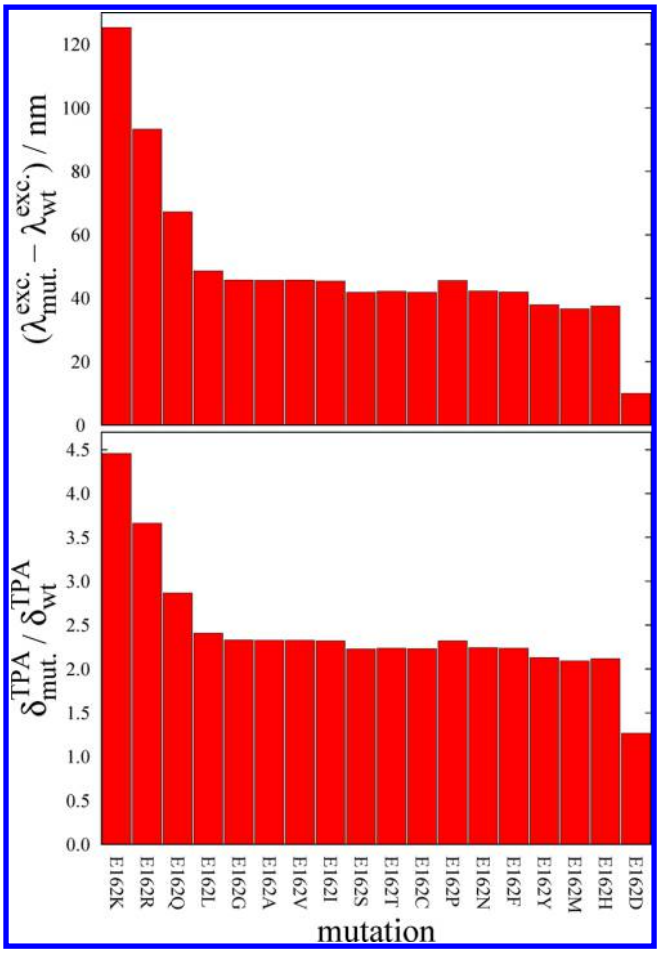

Figure 5. Spectral shifts (up) and TPA transition probability ratios (down) with respect to the wild-type protein for a series of glutamate 162 mutations to other amino acids.

task. The results of the last study are compared with previous experimental and computational studies, and they either reproduce or improve on previous computational results.

In summary, the presented PERI-CC2 TPA implementation provides a useful new tool for the theoretical description of complex photoactive systems.

■ ASSOCIATED CONTENT

Supporting Information

OPA spectra of water-solvated formamide calculated with PERI-CC2, PE-CC2, and PE-CCSD; OPA spectra of water-solvated uracil with and without QM water molecules; and TPA spectra of water solvated formamide and uracil generated from 30, 60, 90, and 120 points. The Supporting Information is available free of charge on the ACS Publications website at DOI: 10.1021/acs.jctc.5b00496.

■ AUTHOR INFORMATION

Corresponding Authors

*(O.C.) Phone: +45 5152 6145. E-mail: ove@chem.au.dk.
*(C.H.) Phone: ++49 (0)234 32 26485. Fax: ++49 (0)234 32 14045. E-mail: christof.haettig@rub.de.

Funding

D.H. acknowledges funding from The Marie Curie ITN, Grant Agreement 2010-264362. O.C. acknowledges support from the Lundbeck Foundation, the Danish e-Infrastructure Cooperation (DeIC), and the Danish Council for Independent Research through a Sapere Aude III grant (DFF4002-00015). This work is also supported by the Cluster of Excellence RESOLV (EXC 1069) funded by the Deutsche Forschungsgemeinschaft (C.H.) and the ERASMUS exchange program (A.M.K.).

Notes

The authors declare no competing financial interest.

■ REFERENCES

(1) Göppert-Mayer, M. *Ann. Phys. (Berlin, Ger.)* **1931**, *401*, 273−294.
(2) Kaiser, W.; Garrett, C. G. B. *Phys. Rev. Lett.* **1961**, *7*, 229−231.
(3) Denk, W.; Strickler, J.; Webb, W. *Science* **1990**, *248*, 73−76.
(4) Stellacci, F.; Bauer, C.; Meyer-Friedrichsen, T.; Wenseleers, W.; Alain, V.; Kuebler, S.; Pond, S.; Zhang, Y.; Marder, S.; Perry, J. *Adv. Mater.* **2002**, *14*, 194−198.
(5) Hopper, C. *Lancet Oncol.* **2000**, *1*, 212−219.
(6) Fisher, W. G.; Partridge, W. P.; Dees, C.; Wachter, E. A. *Photochem. Photobiol.* **1997**, *66*, 141−155.
(7) Helmchen, F.; Denk, W. *Nat. Methods* **2005**, *2*, 932−940.
(8) Theer, P.; Hasan, M. T.; Denk, W. *Opt. Lett.* **2003**, *28*, 1022−1024.
(9) Denk, W.; Delaney, K.; Gelperin, A.; Kleinfeld, D.; Strowbridge, B.; Tank, D.; Yuste, R. *J. Neurosci. Methods* **1994**, *54*, 151−162.
(10) Maruo, S.; Nakamura, O.; Kawata, S. *Opt. Lett.* **1997**, *22*, 132−134.
(11) Wu, E.-S.; Strickler, J. H.; Harrell, W. R.; Webb, W. W. *Proc. SPIE* **1992**, *1674*, 776−782.
(12) Strickler, J. H.; Webb, W. W. *Opt. Lett.* **1991**, *16*, 1780−1782.
(13) So, P. *Opt. Express* **1998**, *3*, 312−314.
(14) McClain, W. M. *Acc. Chem. Res.* **1974**, *7*, 129−135.
(15) Čížek, J. *J. Chem. Phys.* **1966**, *45*, 4256−4266.
(16) Christiansen, O.; Koch, H.; Jørgensen, P. *Chem. Phys. Lett.* **1995**, *243*, 409−418.
(17) Ahlrichs, R. *Phys. Chem. Chem. Phys.* **2004**, *6*, 5119−5121.
(18) Hättig, C.; Weigend, F. *J. Chem. Phys.* **2000**, *113*, 5154−5161.
(19) Nanda, K. D.; Krylov, A. I. *J. Chem. Phys.* **2015**, *142*, 064118.
(20) Gao, J. *J. Comput. Chem.* **1997**, *18*, 1061−1071.
(21) Olsen, J. M. H.; Aidas, K.; Kongsted, J. *J. Chem. Theory Comput.* **2010**, *6*, 3721−3734.
(22) Olsen, J. M. H.; Kongsted, J. *Adv. Quantum Chem.* **2011**, *61*, 107−143.
(23) Sneskov, K.; Schwabe, T.; Kongsted, J.; Christiansen, O. *J. Chem. Phys.* **2011**, *134*, 104108.
(24) Hedegård, E. D.; List, N. H.; Jensen, H. J. A.; Kongsted, J. *J. Chem. Phys.* **2013**, *139*, 044101−1.
(25) Warshel, A.; Levitt, M. *J. Mol. Biol.* **1976**, *103*, 227−249.
(26) Senn, H. M.; Thiel, W. *Angew. Chem., Int. Ed.* **2009**, *48*, 1198−1229.
(27) Day, P. N.; Jensen, J. H.; Gordon, M. S.; Webb, S. P.; Stevens, W. J.; Krauss, M.; Garmer, D.; Basch, H.; Cohen, D. *J. Chem. Phys.* **1996**, *105*, 1968−1986.
(28) Ghosh, D.; Kosenkov, D.; Vanovschi, V.; Williams, C. F.; Herbert, J. M.; Gordon, M. S.; Schmidt, M. W.; Slipchenko, L. V.; Krylov, A. I. *J. Phys. Chem. A* **2010**, *114*, 12739−12754.
(29) Gordon, M. S.; Fedorov, D. G.; Pruitt, S. R.; Slipchenko, L. V. *Chem. Rev.* **2012**, *112*, 632−672.
(30) Mennucci, B.; Tomasi, J. *J. Chem. Phys.* **1997**, *106*, 5151−5158.
(31) Mennucci, B. *WIREs Comput. Mol. Sci.* **2012**, *2*, 386−404.
(32) Hättig, C.; Christiansen, O.; Jørgensen, P. *J. Chem. Phys.* **1998**, *108*, 8331−8354.
(33) Schwabe, T.; Sneskov, K.; Haugaard Olsen, J. M.; Kongsted, J.; Christiansen, O.; Hättig, C. *J. Chem. Theory Comput.* **2012**, *8*, 3274−3283.
(34) Friese, D. H.; Winter, N. O. C.; Balzerowski, P.; Schwan, R.; Hättig, C. *J. Chem. Phys.* **2012**, *136*, 174106.
(35) Friese, D. H.; Hättig, C.; Ruud, K. *Phys. Chem. Chem. Phys.* **2012**, *14*, 1175−1184.

DOI: 10.1021/acs.jctc.5b00496
J. Chem. Theory Comput. 2015, 11, 3669−3678

(36) Sneskov, K.; Olsen, J. M. H.; Schwabe, T.; Hättig, C.; Christiansen, O.; Kongsted, J. *Phys. Chem. Chem. Phys.* **2013**, *15*, 7567−7576.
(37) Kongsted, J.; Osted, A.; Mikkelsen, K. V.; Christiansen, O. *J. Chem. Phys.* **2003**, *118*, 1620−1633.
(38) Kongsted, J.; Osted, A.; Mikkelsen, K. V.; Christiansen, O. *J. Chem. Phys.* **2003**, *119*, 10519−10535.
(39) Christiansen, O. *Theor. Chem. Acc.* **2006**, *116*, 106−123.
(40) Christiansen, O.; Jørgensen, P.; Hättig, C. *Int. J. Quantum Chem.* **1998**, *68*, 1−52.
(41) List, N. H.; Coriani, S.; Christiansen, O.; Kongsted, J. *J. Chem. Phys.* **2014**, *140*, 224103.
(42) List, N. H.; Coriani, S.; Kongsted, J.; Christiansen, O. *J. Chem. Phys.* **2014**, *141*, 244107.
(43) Hättig, C.; Köhn, A. *J. Chem. Phys.* **2002**, *117*, 6939.
(44) Köhn, A.; Hättig, C. *J. Chem. Phys.* **2003**, *119*, 5021−5036.
(45) *TURBOMOLE*, v6.6; TURBOMOLE GmbH: Karlsruhe, Germany, 2014. http://www.turbomole.com.
(46) Aidas, K.; Angeli, C.; Bak, K. L.; Bakken, V.; Bast, R.; Boman, L.; Christiansen, O.; Cimiraglia, R.; Coriani, S.; Dahle, P.; Dalskov, E. K.; Ekström, U.; Enevoldsen, T.; Eriksen, J. J.; Ettenhuber, P.; Fernández, B.; Ferrighi, L.; Fliegl, H.; Frediani, L.; Hald, K.; Halkier, A.; Hättig, C.; Heiberg, H.; Helgaker, T.; Hennum, A. C.; Hettema, H.; Hjertenæs, E.; Høst, S.; Høyvik, I.-M.; Iozzi, M. F.; Jansík, B.; Jensen, H. J. A.; Jonsson, D.; Jørgensen, P.; Kauczor, J.; Kirpekar, S.; Kjærgaard, T.; Klopper, W.; Knecht, S.; Kobayashi, R.; Koch, H.; Kongsted, J.; Krapp, A.; Kristensen, K.; Ligabue, A.; Lutnæs, O. B.; Melo, J. I.; Mikkelsen, K. V.; Myhre, R. H.; Neiss, C.; Nielsen, C. B.; Norman, P.; Olsen, J.; Olsen, J. M. H.; Osted, A.; Packer, M. J.; Pawlowski, F.; Pedersen, T. B.; Provasi, P. F.; Reine, S.; Rinkevičius, Ž.; Ruden, T. A.; Ruud, K.; Rybkin, V. V.; Sałek, P.; Samson, C. C. M.; de Merás, A. S.; Saue, T.; Sauer, S. P. A.; Schimmelpfennig, B.; Sneskov, K.; Steindal, A. H.; Sylvester-Hvid, K. O.; Taylor, P. R.; Teale, A. M.; Tellgren, E. I.; Tew, D. P.; Thorvaldsen, A. J.; Thøgersen, L.; Vahtras, O.; Watson, M. A.; Wilson, D. J. D.; Ziolkowski, M.; Ågren, H. *WIREs Comput. Mol. Sci.* **2014**, *4*, 269−284.
(47) Dunning, T. H. *J. Chem. Phys.* **1989**, *90*, 1007−1023.
(48) Weigend, F.; Köhn, A.; Hättig, C. *J. Chem. Phys.* **2002**, *116*, 3175−3183.
(49) Hättig, C. Available from the basis set echange library at https://bse.pnl.gov/bse/portal.
(50) Schuchardt, K. L.; Didier, B. T.; Elsethagen, T.; Sun, L.; Gurumoorthi, V.; Chase, J.; Li, J.; Windus, T. L. *J. Chem. Inf. Model.* **2007**, *47*, 1045−1052.
(51) Frisch, M. J.; Trucks, G. W.; Schlegel, H. B.; Scuseria, G. E.; Robb, M. A.; Cheeseman, J. R.; Scalmani, G.; Barone, V.; Mennucci, B.; Petersson, G. A.; Nakatsuji, H.; Caricato, M.; Li, X.; Hratchian, H. P.; Izmaylov, A. F.; Bloino, J.; Zheng, G.; Sonnenberg, J. L.; Hada, M.; Ehara, M.; Toyota, K.; Fukuda, R.; Hasegawa, J.; Ishida, M.; Nakajima, T.; Honda, Y.; Kitao, O.; Nakai, H.; Vreven, T.; Montgomery, J. A., Jr.; Peralta, J. E.; Ogliaro, F.; Bearpark, M.; Heyd, J. J.; Brothers, E.; Kudin, K. N.; Staroverov, V. N.; Kobayashi, R.; Normand, J.; Raghavachari, K.; Rendell, A.; Burant, J. C.; Iyengar, S. S.; Tomasi, J.; Cossi, M.; Rega, N.; Millam, J. M.; Klene, M.; Knox, J. E.; Cross, J. B.; Bakken, V.; Adamo, C.; Jaramillo, J.; Gomperts, R.; Stratmann, R. E.; Yazyev, O.; Austin, A. J.; Cammi, R.; Pomelli, C.; Ochterski, J. W.; Martin, R. L.; Morokuma, K.; Zakrzewski, V. G.; Voth, G. A.; Salvador, P.; Dannenberg, J. J.; Dapprich, S.; Daniels, A. D.; Farkas, O.; Foresman, J. B.; Ortiz, J. V.; Cioslowski, J.; Fox, D. J. *Gaussian 09*, revision A.01; Gaussian, Inc.: Wallingford, CT, 2009.
(52) Hršak, D.; Holmegaard, L.; Poulsen, A. S.; List, N. H.; Kongsted, J.; Denofrio, M. P.; Erra-Balsells, R.; Cabrerizo, F. M.; Christiansen, O.; Ogilby, P. R. *Phys. Chem. Chem. Phys.* **2015**, *17*, 12090−12099.
(53) Miller, D. L.; Weinstock, M. A. *J. Am. Acad. Dermatol.* **1994**, *30*, 774−778.
(54) Crespo-Hernández, C. E.; Cohen, B.; Hare, P. M.; Kohler, B. *Chem. Rev.* **2004**, *104*, 1977−2020.
(55) Callis, P. R. *Annu. Rev. Phys. Chem.* **1983**, *34*, 329−357.
(56) Voet, D.; Gratzer, W. B.; Cox, R. A.; Doty, P. *Biopolymers* **1963**, *1*, 193−208.
(57) Clark, L. B.; Peschel, G. G.; Tinoco, I. *J. Phys. Chem.* **1965**, *69*, 3615−3618.
(58) Improta, R.; Barone, V. *J. Am. Chem. Soc.* **2004**, *126*, 14320−14321.
(59) Fleig, T.; Knecht, S.; Hättig, C. *J. Phys. Chem. A* **2007**, *111*, 5482−5491.
(60) Gustavsson, T.; Bányász, Á; Lazzarotto, E.; Markovitsi, D.; Scalmani, G.; Frisch, M. J.; Barone, V.; Improta, R. *J. Am. Chem. Soc.* **2006**, *128*, 607−619.
(61) Zazza, C.; Amadei, A.; Sanna, N.; Grandi, A.; Chillemi, G.; Di Nola, A.; D'Abramo, M.; Aschi, M. *Phys. Chem. Chem. Phys.* **2006**, *8*, 1385−1393.
(62) Olsen, J. M.; Aidas, K.; Mikkelsen, K. V.; Kongsted, J. *J. Chem. Theory Comput.* **2010**, *6*, 249−256.
(63) Epifanovsky, E.; Kowalski, K.; Fan, P.-D.; Valiev, M.; Matsika, S.; Krylov, A. I. *J. Phys. Chem. A* **2008**, *112*, 9983−9992.
(64) Ludwig, V.; Coutinho, K.; Canuto, S. *Phys. Chem. Chem. Phys.* **2007**, *9*, 4907−4912.
(65) Nagel, G.; Ollig, D.; Fuhrmann, M.; Kateriya, S.; Musti, A. M.; Bamberg, E.; Hegemann, P. *Science* **2002**, *296*, 2395−2398.
(66) Sineshchekov, O. A.; Jung, K.-H.; Spudich, J. L. *Proc. Natl. Acad. Sci. U. S. A.* **2002**, *99*, 8689−8694.
(67) Suzuki, T.; Yamasaki, K.; Fujita, S.; Oda, K.; Iseki, M.; Yoshida, K.; Watanabe, M.; Daiyasu, H.; Toh, H.; Asamizu, E.; Tabata, S.; Miura, K.; Fukuzawa, H.; Nakamura, S.; Takahashi, T. *Biochem. Biophys. Res. Commun.* **2003**, *301*, 711−717.
(68) Boyden, E. S.; Zhang, F.; Bamberg, E.; Nagel, G.; Deisseroth, K. *Nat. Neurosci.* **2005**, *8*, 1263−1268.
(69) Fenno, L.; Yizhar, O.; Deisseroth, K. *Annu. Rev. Neurosci.* **2011**, *34*, 389−412.
(70) Dawydow, A.; Gueta, R.; Ljaschenko, D.; Ullrich, S.; Hermann, M.; Ehmann, N.; Gao, S.; Fiala, A.; Langenhan, T.; Nagel, G.; Kittel, R. J. *Proc. Natl. Acad. Sci. U. S. A.* **2014**, *111*, 13972−13977.
(71) Rickgauer, J. P.; Tank, D. W. *Proc. Natl. Acad. Sci. U. S. A.* **2009**, *106*, 15025−15030.
(72) Kato, H. E.; Zhang, F.; Yizhar, O.; Ramakrishnan, C.; Nishizawa, T.; Hirata, K.; Ito, J.; Aita, Y.; Tsukazaki, T.; Hayashi, S.; Hegemann, P.; Maturana, A. D.; Ishitani, R.; Deisseroth, K.; Nureki, O. *Nature* **2012**, *482*, 369−374.
(73) Inaguma, A.; Tsukamoto, H.; Kato, H. E.; Kimura, T.; Ishizuka, T.; Oishi, S.; Yawo, H.; Nureki, O.; Furutani, Y. *J. Biol. Chem.* **2015**, *290*, 11623−11634.
(74) Berndt, A.; Schoenenberger, P.; Mattis, J.; Tye, K. M.; Deisseroth, K.; Hegemann, P.; Oertner, T. G. *Proc. Natl. Acad. Sci. U. S. A.* **2011**, *108*, 7595−7600.
(75) Gunaydin, L. A.; Yizhar, O.; Berndt, A.; Sohal, V. S.; Deisseroth, K.; Hegemann, P. *Nat. Neurosci.* **2010**, *13*, 387−392.

DOI: 10.1021/acs.jctc.5b00496
J. Chem. Theory Comput. 2015, 11, 3669−3678